Journal of the Korean Society
for Nondestructive Testing
Vol. 28, No. 3 (2008. 6)

Advances in Ultrasonic Testing of Austenitic Stainless Steel Welds

J. Moysan*†, M. A. Ploix*, G. Corneloup*, P. Guy**, R. El Guerjouma*** and B. Chassignole****

Abstract A precise description of the material is a key point to obtain reliable results when using wave propagation codes. In the case of multipass welds, the material is very difficult to describe due to its anisotropic and heterogeneous properties. Two main advances are presented in the following. The first advance is a model which describes the anisotropy resulting from the metal solidification and thus the model reproduces an anisotropy that is correlated with the grain orientation. The model is called MINA for modelling anIsotropy from Notebook of Arc welding. With this kind of material modelling a good description of the behaviour of the wave propagation is obtained, such as beam deviation or even beam division. But another advance is also necessary to have a good amplitude prediction: a good quantification of the attenuation, particularly due to grain scattering, is also required as far as attenuation exhibits a strong anisotropic behaviour too. Measurement of attenuation is difficult to achieve in anisotropic materials. An experimental approach has been based both on the decomposition of experimental beams into plane waves angular spectra and on the propagation modelling through the anisotropic material via transmission coefficients computed in generally triclinic case. Various examples of results are showed and also some prospects to continue refining numerical simulation of wave propagation.

Keywords: Austenitic Weld, Anisotropy, Grain Orientation, Ultrasonic Propagation Modelling, Beam Deviation, Attenuation

1. Introduction

Welds made in austenitic steel show a heterogeneous and anisotropic structure that causes phenomena of diffusion, attenuation and deviation of the ultrasonic beam which make interpretation of testing difficult. Increasing the knowledge to be able to predict the ultrasonic testing of stainless welds was an international large and long term research field. Some years ago works aiming at giving a precise description of the material gave significant progresses (Chassignole et al., 2000). This idea was carried on by increasing the quality of the material description using knowledge on the solidification mechanisms in multipass welds (Corneloup et al,. 2001). This study presents two major advances for the understanding of ultrasonic testing of welds. All these studies were supported by EDF (French Electricity Board).

Information available in the welding notebook is firstly presented to explain how weld passes could be modeled. Validation of this model is obtained by comparing local grain orientations predicted by the model and those measured on the corresponding weld macrographs. The coupling with a finite element code allows comparing simulated and

Received: May 7, 2008, Revised: June 13, 2008, Accepted: June 17, 2008. * Laboratoire de Caractérisation Non Destructive, Université de la Méditerranée, IUT Aix en Provence, 13625 Aix en Provence, France, ** Laboratoire MATEIS, INSA Lyon, 7 Avenue Jean Capelle, 69621 Villeurbanne, France, *** LAUM, Avenue Olivier Messiaen, 72085 Le Mans Cedex 9, France, **** Département MMC, EDF R&D, Site des Renardières, 77818 Moret-sur-Loing, France, † Corresponding author: joseph.moysan@univmed.fr

experimental signals. These last results demonstrate the effectiveness of this approach. In a second part of this study, the improvement of the material description is achieved by developing a complete approach to obtain precise attenuation values for this kind of welds.

2. Fundamentals of the MINA Model

When a transversal macrograph of a multipass weld is analysed, it can be noticed that the grains show multiple directions, more often without symmetry. The study of several macrographs of flat position welds shows that grain orientation depends on the order of weld passes sequence. The MINA model was developed for welds made with a shielded electrode. This order of pass deposition is written down in the welding book (see Fig. 1) with other information such as the number of passes, the diameter of electrodes and the geometry of the initial chamfer. Physical phenomena affecting the crystalline growth during multi-pass welding are numerous and are widely detailed in the literature (Rappaz et al., 1995; Kurz, 1995; Limmaneevichitr et Kou, 2000): solidification, crystalline growth, convection, temperature gradient, Marangoni's effect. Some parameters can be unknown in details in the case of manual arc welding. The MINA model (Modelling anIsotropy from Notebook of Arc welding) does not simulate grains growth but predicts the result of the grain growth (Moysan et al., 2003). Knowing the grain orientation is a key point for input data of material description into wave propagation code.

2.1 Physical Phenomena Governing Grain Growth in Austenitic Stainless Steel Welds

The grains grow by solidification, from the bottom to the top of the weld, and from the bottom to the top of a pass. Their growth is governed by three physical phenomena : the epitaxial growth, the influence of temperature gradient, and the competition between the grains(selective growth).

Epitaxial growth during welding implies that the melt metal takes in each point the cristallographic orientations of the underlying pass. The grain shape can also take turns during the growth but the cristallographic orientation is always kept.

When the temperature gradient changes of direction, the grain shape tends to align as much as possible with the gradient direction. Then grains can take slight turns to follow the gradient direction. In the case of multi-pass welding, the direction of the temperature gradient changes within the welding pass and also from one pass to the other.

There is a competition between grains as they preferentially grow if their longitudinal axis is close to the direction of the temperature gradient. A grain whose axis is very far from the gradient will be stopped and stranded in its

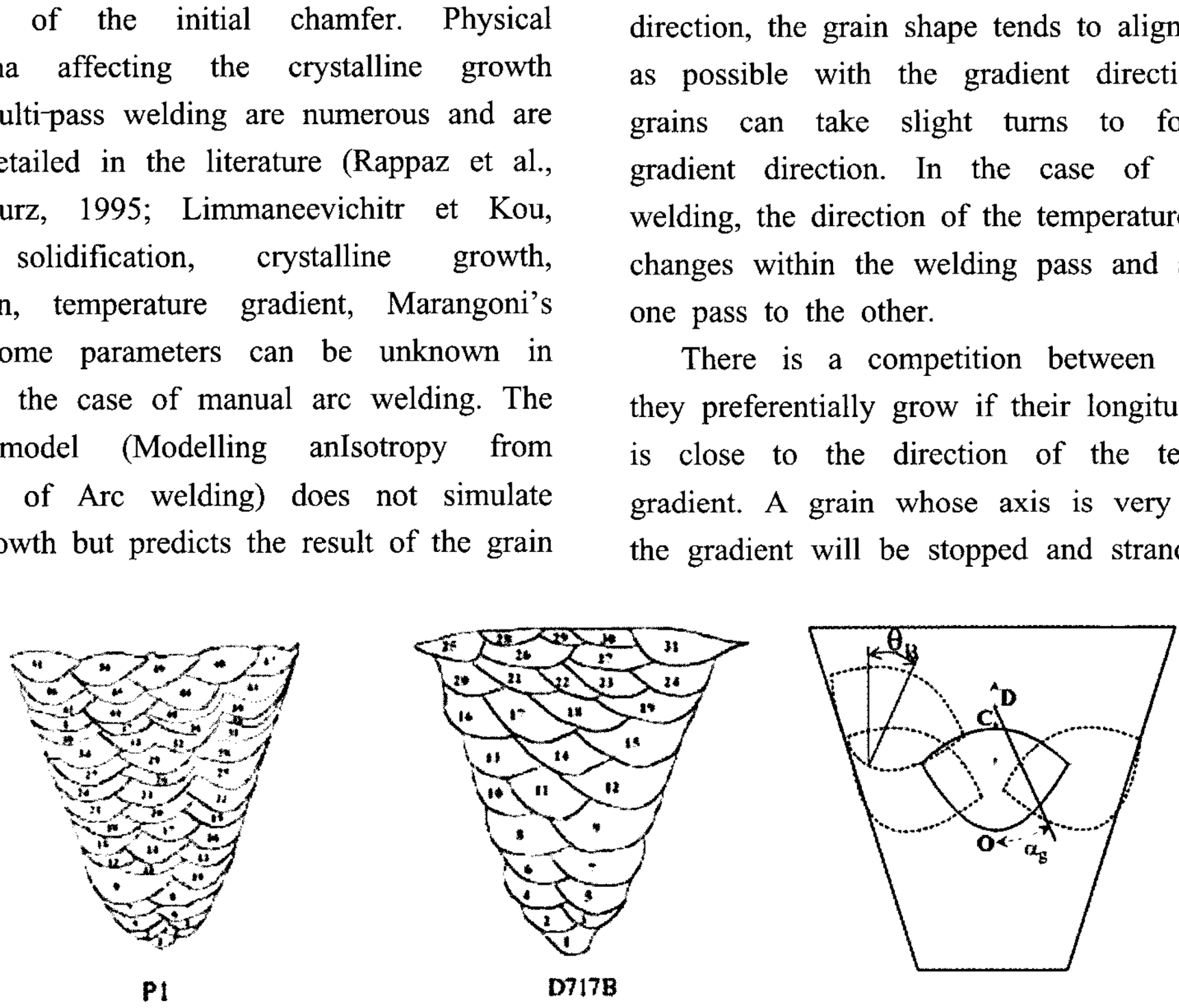

(Examples of realisations by two different welders on a same geometry)

Fig. 1 Exemple of succession of passes described on a welding notebook

growth by better oriented grains.

2.2 Model Definition

MINA model output is a matrix whose elements represent the local discretized orientation of the grains resulting from the complete solidification process due to the remelting of passes (see Fig. 2(b)). The orientation of a vertical grain is 90°. The corresponding surface of each element could be adapted to the wave propagation (detailed in §4). The matrix size corresponds to the chamfer dimensions written down in the welding book. The matrix elements are filled pass after pass in the real chronological welding order written down in the book.

A pass is represented in the MINA model by a parabolic shape, the scanning being too weak to have convective effects (Marangoni's effects). Pass heights are calculated proportionally to the diameters of the electrodes. It is assumed that the symmetry of simulated temperature gradient is not modified by convective effects of the melting liquid.

A partial remelting is created when a new pass is laid (see Fig. 1(c)). The lateral and vertical remelting rates are respectively noted R_L and R_V. These two parameters, R_L and R_V, are the most important ones and will be obtained by analysis of macrographs of several welds.

Two other parameters are defined to reproduce the operator's skill in relation to the geometry of the welded joint as he can tilt the electrode more or less. This causes an incline of the welding pool. Fig. 1 clearly shows that the passes of concave shape are not simply aligned vertically. In a first approach it is assumed that this phenomenon can be simply described by rotating the direction of temperature gradient without changing the geometric shape of the pass. Two cases are taken into account depending whether the considered pass leans on the chamfer or on a previous pass. When a pass leans on the chamfer the angle of rotation is noted θ_B, it reproduces the influence of the weld geometric shape (Fig. 1(c)). When a pass leans on a previous pass (ex: pass no. 21 of Fig. 1(b)), the temperature gradient is rotated by an angle noted θ_C lower than the observed angle when a pass leans on the chamfer. When a pass leans to its left and its right on other passes (ex: pass no. 28 of Fig. 1(b)), the temperature gradient is symmetric with respect to the vertical line ($\theta_C = 0$). All these angles are automatically calculated in relation to the location of each pass written in the welding notebook.

With these four parameters and the pass parabolic geometry, the grain orientation α_n in a mesh (or element) is calculated using an algorithm which reproduces the three physical phenomena previously mentioned. α_0 denotes the orientation of the grains in the lower element. The angle $\alpha_{gradient}$ represents the temperature gradient direction (Fig. 1(c)). To simulate the slow convergence of a grain orientation from the initial direction towards the temperature gradient direction, and also to simulate the selective growth, an iterative formula is used to weight gradient orientation influence. The number n of iterations for 0.5×0.5 mm² element is a modelling parameter and is material dependant. Following equations indicate the iterative calculus of the grain direction:

$$n = 1, \quad \alpha_{(0)} = \alpha_{lowerbox} \tag{1}$$

$$t_{(n)} = \cos(\alpha_{(n-1)} - \alpha_{gradient}) \tag{2}$$

$$\alpha_{(n)} = t_{(n)}\alpha_{(n-1)} + (1 - t_{(n)})\alpha_{gradient} \tag{3}$$

If a grain is initially oriented far from the temperature gradient, the parameter $t_{(n)}$ tends towards 0 and $(1- t_{(n)})$ tends towards 1, so $\alpha_{(n)}$ tends very quickly towards $\alpha_{gradient}$. It reproduces the selective growth that eliminates the ill-oriented grains in relation to the temperature gradient. When a grain is oriented closer to the temperature gradient, the parameter $t_{(n)}$ tends towards 1, so $\alpha_{(n)}$ remains close to $\alpha_{(n-1)}$ while

taking a slow turn towards the temperature gradient. The more the formula is applied for 0.5×0.5 mm² element, the more quickly the grain tends towards the temperature gradient.

3. Comparisons of Modelled Grain Orientations with Macrographs

The quantification of the MINA parameters is based on macrographs of six welds. All of them are made on the same joint geometry. Among the six, three were made by a first operator (D 717 A, D 717 C, D 717 D) and the others (P1, P2, P3) by another operator. It allows analyzing variations in a manual operation. The two welders chose to perform a more or less pronounced weaving motion of the electrode. This motion is however limited to three times the diameter of the electrode.

Fig. 2 presents results with a mesh-size of 2×2 mm². Fig. 2(a) shows the macrograph, Fig. 2(b) shows the grain orientations, and Fig. 2(c) plots the map of orientation differences. In Fig. 2(c) the differences are presented with level lines where grain orientations are gathered by about twenty degrees. The real grain orientations are measured by an image analysis system.

The comparison is very satisfactory as far as a good correlation between the two figures is noticed. The average error calculated on the whole six welds is about 10° (9,9° and 14° for average error in the two welds presented in Figs. 2). There are areas on the weld where errors are very weak (less than 5°) and some localised areas where the error is more important.

The method is based on the information written in the welding book. It has been proved that the modelling is accurate enough to detect possible errors in the welding book. In such cases grain orientation simulations do not correspond to the macrograph and error goes higher than 22° (Fig. 3). The order of passes is modified by reversing it.

The next step to validate the MINA model is first to demonstrate that the material description allows good finite element modelling of the wave propagation and second to compare this modelling with experimental results.

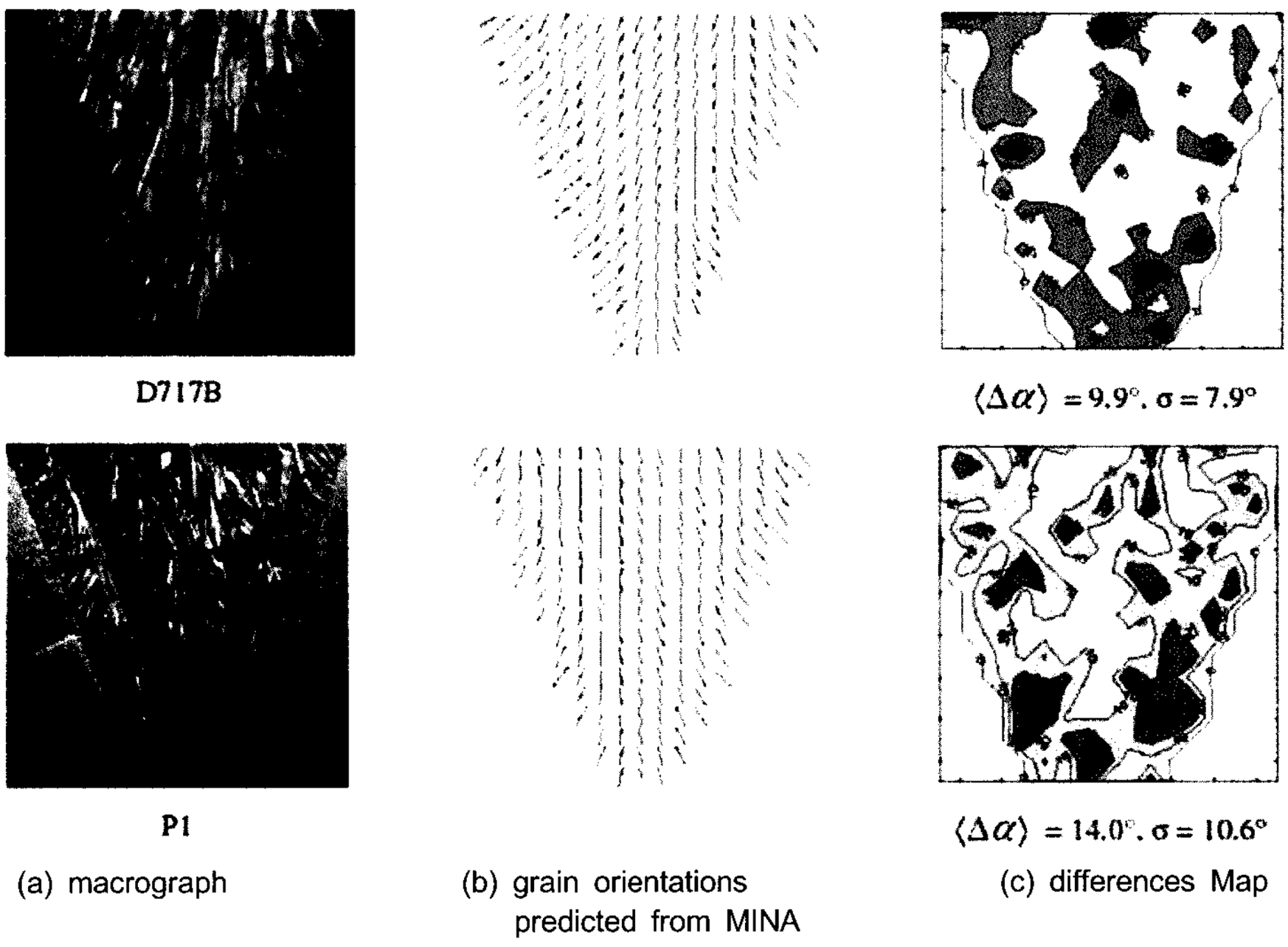

(a) macrograph (b) grain orientations predicted from MINA (c) differences Map

Fig. 2 Comparison of predicted grains from MINA with optically measured orientations

4. Wave Propagation Modelling with Finite Element Code

The MINA model describes the weld and its local anisotropy at a 2 mm scale which is reputed to be a sufficient discretization for a good ultrasonic testing simulation. The output of the grain orientation model is designed to be incorporated into the finite element code ATHENA 2D. This code was developed by EDF and INRIA (Becache et al 2000.). It simulates the propagation of ultrasonic waves through anisotropic and heterogeneous media. The code solves the elastodynamic equations in a transitory regime. With the hypothesis of small deformations the equations are given by:

$$\rho \frac{\partial^2 u}{\partial t^2} - div\sigma(u) = f \tag{4}$$

where ρ is the density, σ is the stress tensor, u is the particle displacement and f is a strength source. In Hooke's law $\sigma_{ij} = C^{\alpha}_{ijkl}\varepsilon_{kl}$, ε is the strain tensor and C^{α} is the elasticity coefficients tensor. Index α indicates that the coordinate system, in which the elasticity coefficients are expressed, depends on the grain orientation. With $A^{\alpha} = (C^{\alpha})^{-1}$ and $v = \frac{\partial u}{\partial t}$ (particle velocity) elastodynamics equations can be written in the form of a first order hyperbolic system whose unknown factors are the particle velocity $\underline{v}$ and the stress σ:

$$\begin{cases} \rho \dfrac{\partial v}{\partial t} - \mathrm{div}\sigma = f \\ A^{\alpha} \dfrac{\partial \sigma}{\partial t} - \varepsilon = 0 \end{cases} \tag{5}$$

ATHENA uses the perfectly adapted absorbing layers (PML) to define the boundaries of the calculation domain without creating reflections on the domain limits.

Simulations are performed using a transmission technique to simplify the testing

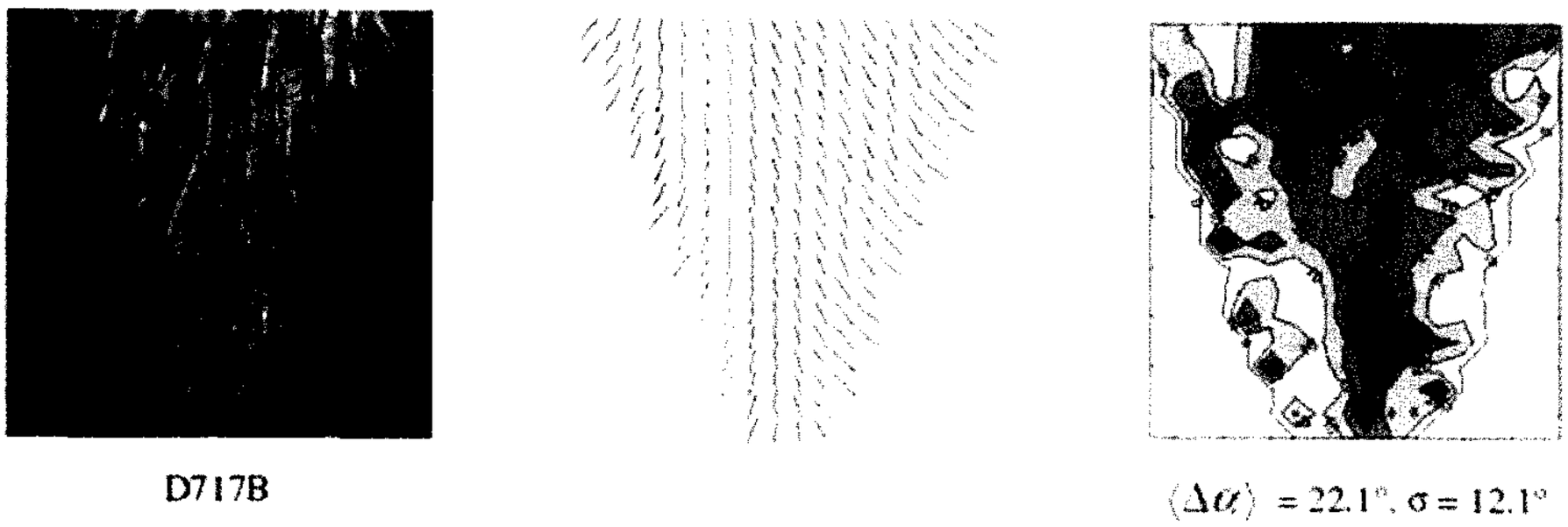

Fig. 3 Simulations for a wrong order of passes

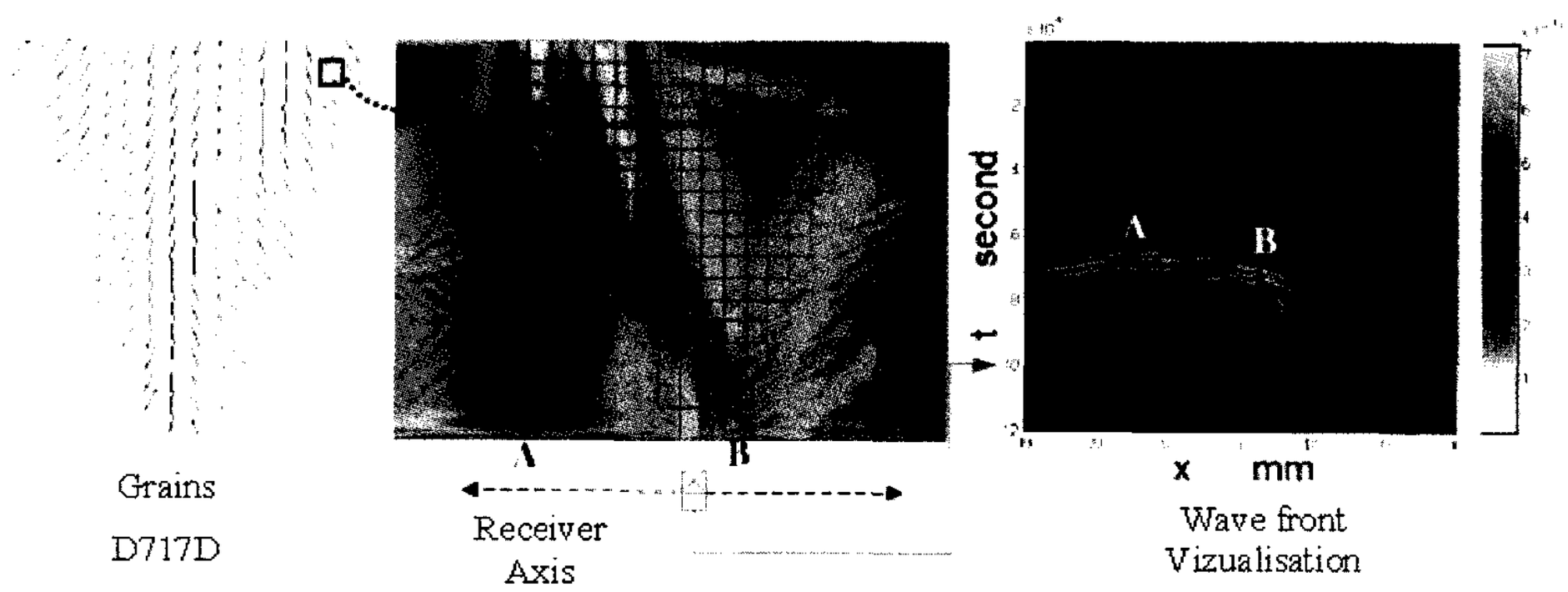

Fig. 4 General description of the simulation with ATHENA code

modelling (Apfel et al., 2005). A heterogeneous anisotropic structure is defined by introducing a mesh containing the grain orientations. This permits to calculate elasticity coefficients with appropriate coordinate systems at any point of the weld. A summary of the coupling between ATHENA and MINA is presented on Fig. 4. In this figure the transducer generates a beam of longitudinal waves with normal incidence and it is located at x = -12 mm from the middle position of the weld. Maximum values reached by particles velocity at each point of the mesh are calculated. The code can provide temporal representation of the wave propagation (on the right part of Fig. 4) or the global description of the beam (on the middle part of Fig. 4). To compare experimental and simulated results, the receiver is placed at the bottom of the weld (experiment in transmission mode in water). The corresponding echodynamic curves are calculated using ATHENA results in transmission at the bottom of the weld.

Effects of the weld anisotropy are visible on this Fig. 4: a deformation and an important skewing of the ultrasonic beam are observed. In the case of isotropic steel this field would be symmetrical without any skewing or deformation. Fig. 5 represents three echodynamic curves. The first one results from ATHENA simulation with MINA grain structure. The second one is calculated with ATHENA and the real grains structure (from macrograph). And the third curve is the experimental one. The relative amplitudes and positions of the peaks simulated by ATHENA are good between the two implemented grain structures. This confirms the interest of coupling these two models. It confirms also that the scale of modelling is correct for this category of welds and for this range of frequency (Apfel et al., 2005). In comparison with experimental results, peaks positions are correctly predicted but there are differences in amplitudes. The origin of these differences is the real attenuation which is not reproduced with the finite element modelling. For such columnar grains structures the attenuation can reach 0.3 dB/mm (Seldis, 1998). The next advance is consequently a progress in the description of the attenuation. It requires both a progress in the finite element code and a precise knowledge of the attenuation in austenitic stainless steel with elongated grains.

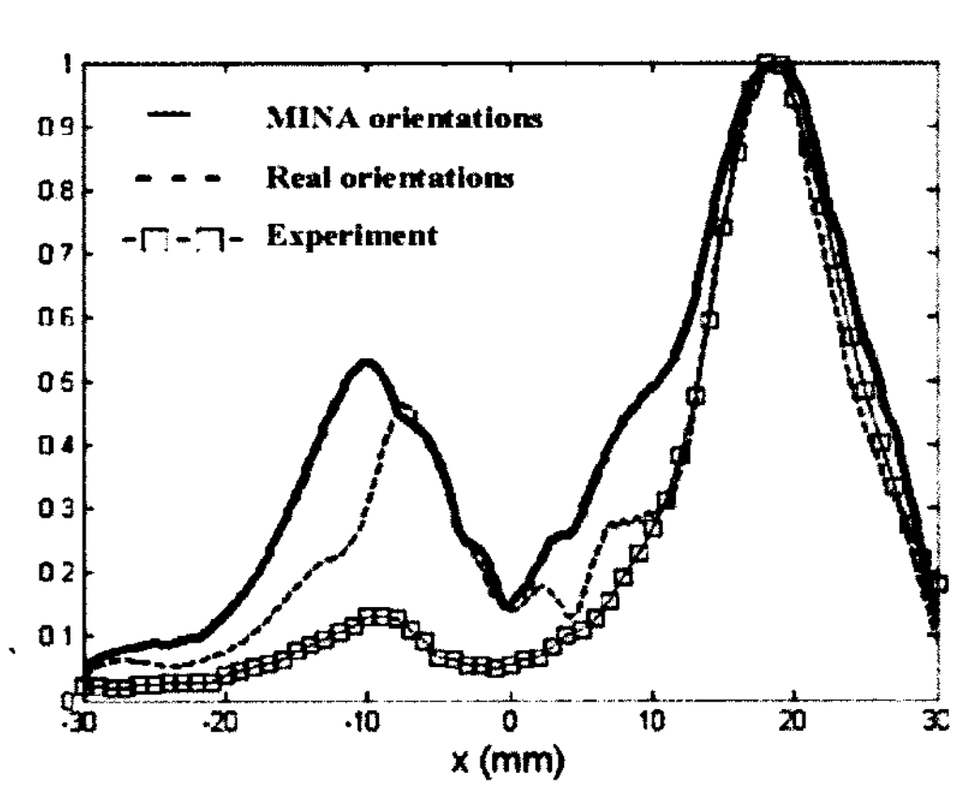

Fig. 5 Examples of echodynamic curves

5. Introducing Attenuation into the Wave Propagation Code

Attenuation in such welded materials is mainly caused by the scattering effect on the columnar grains. The value of this attenuation depends on the size, shape and orientation of the grains but also on their anisotropy. An experimental setup is defined in order to study the ultrasonic attenuation as a function of the grain orientation (Ploix et al., 2006).

The welded samples used for the experiments were cut in a flat position and shielded metal arc welding mock-up. The samples can then be considered macroscopically homogeneous and orthotropic. The real orientations that are obtained are 0°, 10°, 35°, 45°, 60°, 80° and 85° relatively to the normal to the sample surface.

Experimental setup is a classical measurement in transmission using an immersion tank. The emitter is a 1/2" in diameter piezoelectric wideband transducer of 2.25 MHz central frequency, and the receiver is a hydrophone. The sample is

placed in the farfield of the emitter. The beam decomposition into plane waves angular spectrum is used to correct the beam divergence.

The hydrophone scans a plane $z=z_o$ parallel to the emitter surface and acquires a signal $s(t,x,y,z_o)$ at each point (x,y) of the plane. The angular frequency spectrum $S(x,y,\omega_o,z_o)$ is calculated for each signal by Fourier-transform. For an angular frequency ω_o, a 2D spatial Fourier-transform gives the so called plane waves angular spectrum $U(k_x,k_y,\omega_o,z_o)$ in the k-space domain (Ploix et al., 2006).

Two different planes are scanned. First the incident field is mapped without any sample. The hydrophone moves in the plane containing the front face of the sample ($z_o=0$). Then the sample is inserted and the transmitted field is mapped in a plane in the proximity of the sample's back face ($z_o>d$). For the angular frequency ω_o corresponding to a frequency of 2.25 MHz, the plane waves angular spectra $U(k_x,k_y,\omega_o,z_o=0) = U_{inc}$ and $U(k_x,k_y,\omega_o,z_o=d+\epsilon) = U_{tra}$ are calculated. A "semi-theoretical" transmitted plane waves angular spectrum U'_{tra} is obtained by multiplying experimental U_{inc} with the transmission coefficients calculated in the k-space domain.

Transmission coefficients are calculated by solving the Christoffel equation with the corresponding boundary conditions at each interface. The problem of transmission coefficients computation was solved in the orthotropic case (Hosten, 1991) and was then extended to the monoclinic case. The elastic description of an orthotropic material disorientated according to an axis of the fixed coordinate system becomes monoclinic. So, except for samples with 0° and 90° grain orientation that present an orthotropic description, all other samples are described as monoclinic material.

The Fig. 6 represents some experimental maps of the transmitted beams through samples (peak-to-peak amplitudes). The circle represents the position of the incident beam at the first interface. For some samples a deviation in two directions is observed (sample 0°). At 45° there is no deviation as expected by theory (Hirsekorn 1986). If the two deviations are considered, the material exhibits triclinic elastic properties for the ultrasonic beam. Transmitted coefficients should be calculated for this case (Ploix et al., 2006).

In this approach, deviations and mode conversions are taken into account. The attenuation for each direction of propagation (k_x,k_y) is then obtained by comparing simulated transmitted beam and real ones. The global attenuation is then expressed as the ratio between the experimental transmitted energy E_{tra}^{exp} and the theoretical transmitted energy E_{tra}^{th}:

$$E_{tra}^{th}(\omega_o)=\iint\left|A_{tra}^{exp}(k_2,k_3,\omega_o)\cdot T_{gl}(k_2,k_3,\omega_o)\right|^2 dk_2dk_3 \quad (6)$$

$$E_{tra}^{exp}(\omega_o)=\iint\left|A_{tra}^{exp}(k_2,k_3,\omega_o)\right|^2 dk_2dk_3 \quad (7)$$

$$\alpha(\omega_o)=\frac{10}{d}\log\left(\frac{E_{tra}^{th}(\omega_o)}{E_{tra}^{exp}(\omega_o)}\right) \quad (8)$$

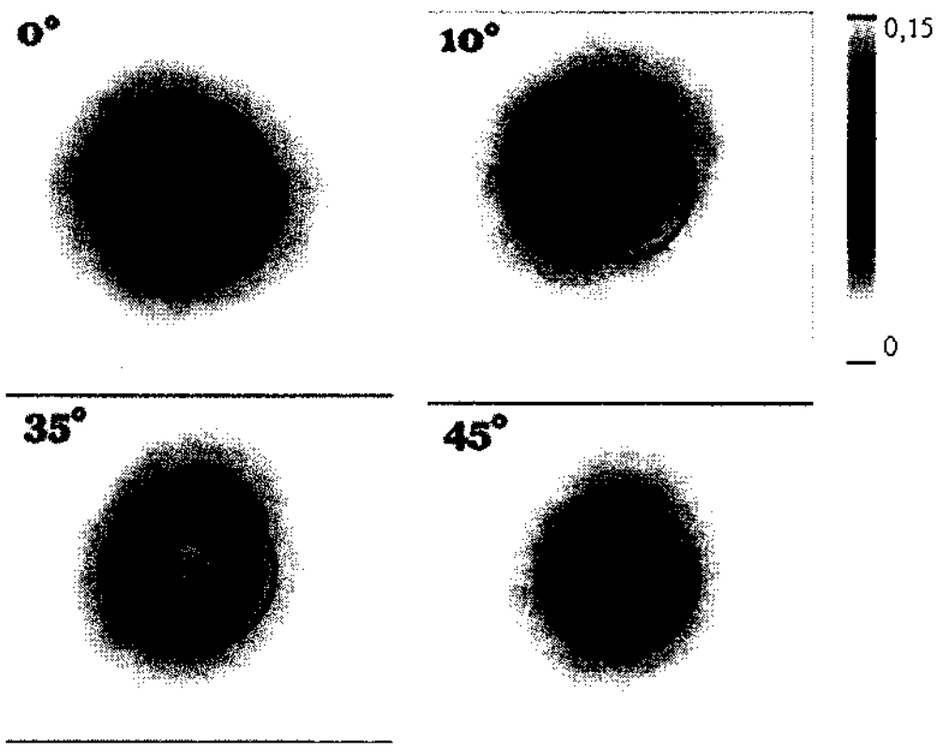

Fig. 6 Beam deviations depending of the incidence angle

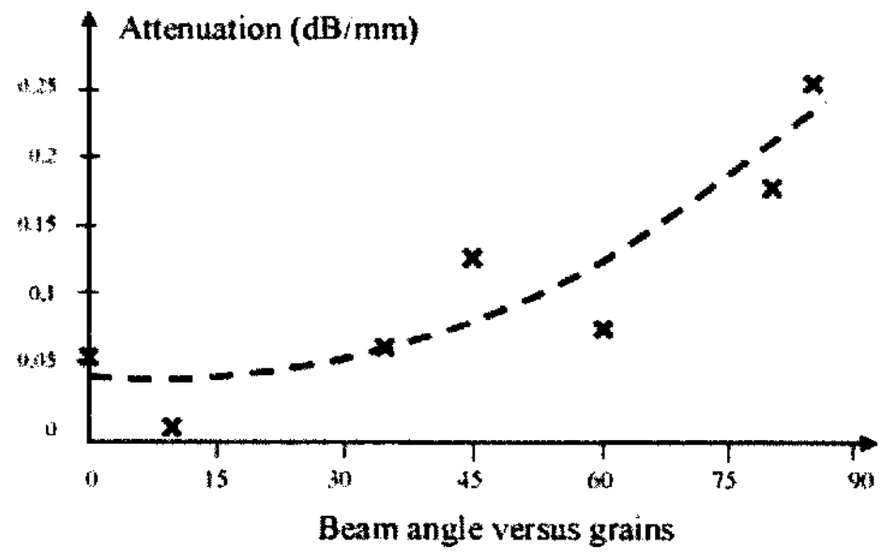

Fig. 7 Experimental results of attenuation

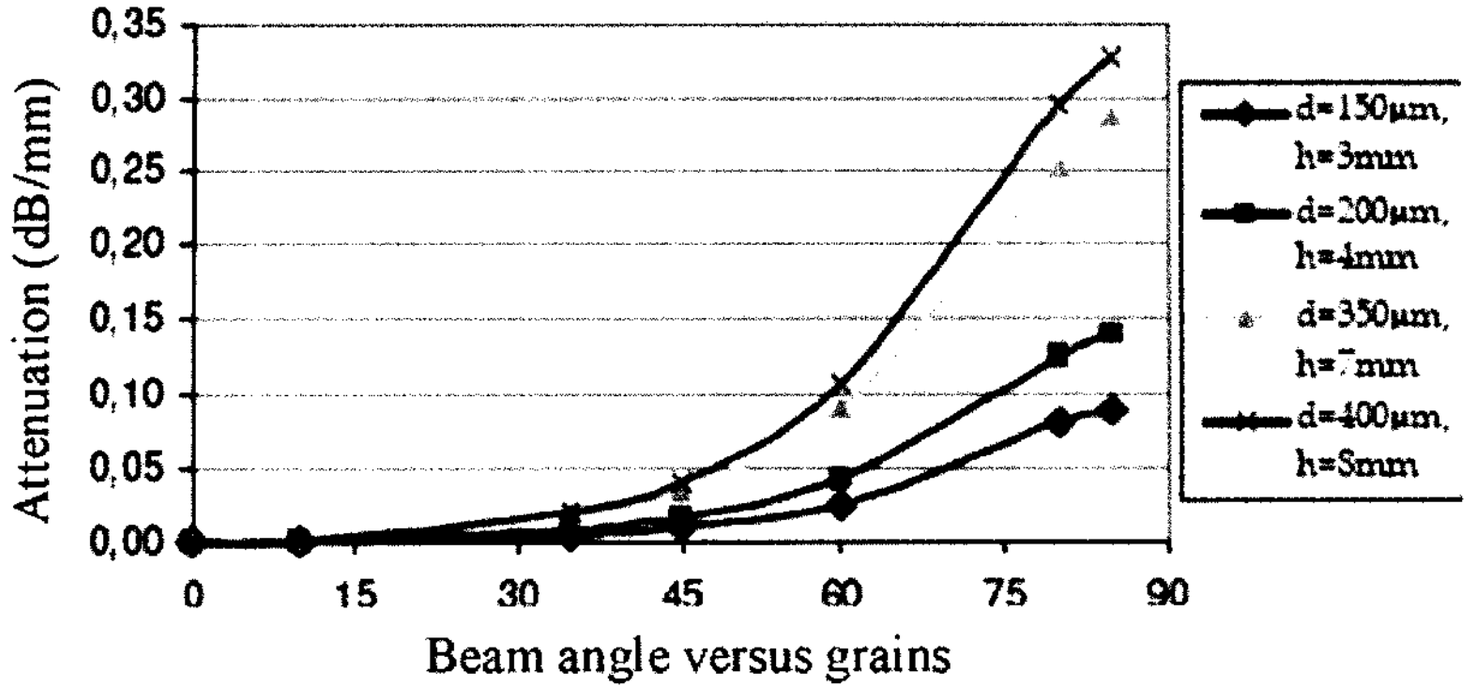

Fig. 8 Attenuation depending on the beam angle versus grains orientation

The experimental results are presented in Fig. 7. The correction of beam deviation in two directions is used to obtain a good transmitted energy. With this correction a global monotonic increase of the attenuation is observed. These experimental results are in good agreement with theoretical calculations using Ahmed's modelling (Ahmed and Thompson 1992, Ahmed and Thompson 1996). In Fig. 8 this modelling is used with parameters (size and shape) adapted to the typical grain structure observed in multipass welds under study. A more precise description of the grain shape distribution would be required to go further in the analysis of these results.

A new development of the ATHENA code allows taking into account the attenuation. It improves modelling tools for heterogeneous material, for example the examination of the branch pipe weld connecting the Chemical and Volume Control System (Chassignole et al. 2007). Preliminary results using attenuation values obtained by Ploix also showed correct predictions of the amplitudes predicted by on echoes reflected by holes after beam propagation through a weld.

6. Conclusion

Two main advances in the field of ultrasonic modelling are presented. They concern the ultrasonic testing of austenitic stainless steel welds which were sometimes reputed to be very difficult to be qualified by ultrasound since various difficulties occurred: complications in the beam prediction (skewing, division), worries in attenuation prediction. The works supported by EDF allows great progresses as far as modelling of ultrasonic testing for these complex structures is now possible. Extensions of the MINA model to other welding techniques may be considered in future works. For example welds made with a refractory electrode (TIG) are also of great interest. These progresses enable to imagine in a next future a complete inverse methodology to reconstruct the true material even if only partial data are known on the welding process.

References

Ahmed, S. and Thompson, R. B. (1992) Effect of Preferred Grain Orientation and Grain Elongation on Ultrasonic Wave Propagation in Stainless Steel, in: D. O. Thompson and D. E. Chimenti (Eds.), *Review of Progress in QNDE 11*, pp. 1999-2006

Ahmed, S. and Thompson, R. B. (1996) Propagation of Elastic Waves in Equiaxed Stainless-steel Polycrystals with Aligned [001] Axes, J. Acoust. Soc. Am. 99, pp. 2086-2096

Apfel, A., Moysan, J., Corneloup, G., Fouquet,

T. and Chassignole, B. (2005) Coupling an Ultrasonic Propagation Code with a Model of the Heterogeneity of Multipass Welds to Simulate the Ultrasonic Testing, Ultrasonics, Vol. 43, Issue 6, pp. 447-456

Becache, E., Joly, P. and Tsogka, C. (2000) An Analysis of New Mixed Finite Elements for the Approximation of Wave Propagation Problems, SIAM Journal on Numerical Analysis, Vol. 37, pp. 1053-1084

Chassignole, B., Paris, O. and Abittan, E. (2007) Ultrasonic Examination of a CVCS Weld, 6th International Conference on NDE in Relation to Structural Integrity for Nuclear and Pressurised Components, Budapest, 8 – 10 October

Chassignole, B., Villard, D., Dubuget, M., Baboux, J. C. and El Guerjouma, R. (2000) Characterization of Austenitic Stainless Steel Welds for Ultrasonic NDT, in: D. O. Thompson and D. E. Chimenti (Eds.), *Review of Progress in QNDE*, Vol. 20, pp. 1325-1332

Corneloup, G., Apfel, A., Aldon, L., Deschaux, F., Migliorini, D., Cervellin, D., Fras, G., Barreau, G., Chassignole, B. and Villard, D. (2001) *CNRIUT Proceedings*, Roanne, pp. 325-334

Hirsekorn, S. (1986) Directional Dependence of Ultrasonic Propagation in Textured Polycrystals, Journal of the Acoustical Society of America, Vol. 79, No. 5, pp. 1269-1279

Hosten, B. (1991) Reflection and Transmission of Acoustic Plane Waves on an Immersed Orthotropic and Viscoelastic Solid Layer, Journal of the Acoustical Society of America, Vol. 89, No. 6, pp. 2745-2752

Kurz, W. (1995) Dendrite Growth in Welding, Mathematical Modelling of Weld Phenomena 2, pp. 41-53

Limmaneevichitr, C. and Kou, S. (2000) Experiments to Simulate Effect of Marangoni Convection on Weld Pool Shape, Welding Research Supplement, August, pp. 231-237

Moysan, J., Apfel, A., Corneloup, G., Chasssignole, B. (2003) Modelling the Grain Orientation of Austenitic Stainless Steel Multipass Welds to Improve Ultrasonic Assessment of Structural Integrity, International Journal of Pressure Vessels and Piping, Vol. 80 No. 2, pp. 77-85

Ploix, M. A., Guy, P., El Guerjouma, R., Moysan, J., Corneloup, J. and Chassignole, B. (2006) Attenuation Assessment for NDT of Austenitic Stainless Steel Welds, 9 th European Conference on NDT, Berlin, 25-29 September

Rappaz, M., Gandin, Ch.-A., Jacot, A. and Charbon, Ch., (1995) Modeling of Microstructure Formation, Modeling of Casting, Welding and Advanced Solidification Processes, Vol. VII, pp. 501-516

Seldis, T., Pecorari, C. and Bieth, M (1998) Measurements of Longitudinal Wave Attenuation in Austenitic Steel, 1st International Conference on NDE in Relation to Structural Integrity for Nuclear and Pressurised Components, Amsterdam (Netherlands), pp. 769-777